



**HAL**  
open science

## Taylor dispersion in a soft channel

Aditya Jha, Masoodah Gunny, Joshua D Mcgraw, Yacine Amarouchene, Thomas Salez

► **To cite this version:**

Aditya Jha, Masoodah Gunny, Joshua D Mcgraw, Yacine Amarouchene, Thomas Salez. Taylor dispersion in a soft channel. 2026. <hal-05581517>

**HAL Id: hal-05581517**

**<https://hal.science/hal-05581517v1>**

Preprint submitted on 6 Apr 2026

**HAL** is a multi-disciplinary open access archive for the deposit and dissemination of scientific research documents, whether they are published or not. The documents may come from teaching and research institutions in France or abroad, or from public or private research centers.

L'archive ouverte pluridisciplinaire **HAL**, est destinée au dépôt et à la diffusion de documents scientifiques de niveau recherche, publiés ou non, émanant des établissements d'enseignement et de recherche français ou étrangers, des laboratoires publics ou privés.



Distributed under a Creative Commons CC BY 4.0 - Attribution - International License

# Taylor dispersion in a soft channel

Aditya Jha,<sup>1,2,\*</sup> Masoodah Gunny,<sup>3,4</sup> Joshua D. McGraw,<sup>3,4</sup> Yacine Amarouchene,<sup>2</sup> and Thomas Salez<sup>2,†</sup>

<sup>1</sup>*TCM Group, Cavendish Laboratory, University of Cambridge, Cambridge CB3 0US, United Kingdom.*

<sup>2</sup>*Univ. Bordeaux, CNRS, LOMA, UMR 5798, F-33405 Talence, France.*

<sup>3</sup>*Gulliver UMR 7083 CNRS, ESPCI-PSL, 10 rue Vauquelin, 75005 Paris, France.*

<sup>4</sup>*IPGG, 6 rue Jean-Calvin, 75005 Paris, France.*

(Dated: April 6, 2026)

Diffusion of a solute along a channel is enhanced by hydrodynamic flow, a phenomenon known as Taylor dispersion. In microfluidic applications, the compliance of the channel boundaries modifies the hydrodynamic flow and thus solutal transport. Here, we develop the theory of solutal dispersion in a soft, axisymmetric channel where the channel walls respond to the hydrodynamic pressure through a Winkler response. By deriving the modified macro-transport equation for the solutal concentration dynamics based on multiple-time-scale analysis, we explore the influence of softness on solutal transport for steady and pulsatile configurations. Our main finding is that softness enhances the effective advection velocity and dispersion coefficient, which might have practical implication in biology and microfluidic technology.

Keywords: low-Reynolds-number flows, microfluidics, elasticity, fluid-structure interactions, Brownian motion, colloids, dispersion.

## I. INTRODUCTION

Transport in microchannels plays a fundamental role in living systems. Our understanding of these small-scale flows in the past few decades has been revolutionised with the advent of improved microfabrication technology aiding microfluidic designs [1, 2]. Specifically, a myriad of important biophysical processes including cellular signalling [3] and chemical reactions [4] can be understood by carefully looking at the dynamics of particles moving inside microchannels. With the emergence and the increased use of soft materials including polymeric gels and elastomers, the channel elasticity and its coupling with the fluid flow has become increasingly important. Flows in deformable channels have been intensively studied over the past decade both experimentally [5–7] and theoretically [8–14] with the aim of characterising the flow-deformation coupling. These studies have characterised the changes to the volumetric flow rate and/or pressure gradients in the channel owing to the softness of the walls. Recent studies have highlighted how this coupling can lead to rectified flow controlled by the wall elasticity [14, 15]. The effect of the non-Newtonian nature of the fluid in such channels has also been studied [16, 17], while pulsatile flows have been suggested as a mechanism for characterising the elasticity of the surrounding walls [14, 18].

The transport of solutes in soft microfluidic channels, where the flow is modified by its coupling with the elasticity of the wall, is expected to be fundamentally different from that in rigid channels. In rigid channels, the diffusive dynamics of the particles is coupled with the advection by the flow, a classical phenomenon called Taylor dispersion or Taylor-Aris dispersion [19–26]. Many studies have extended the scope to other scenarios including the effects of chemical reactions and/or absorption at the wall [4, 27–33], boundary thermal fluctuations [34, 35], non-Newtonian fluid flows [36–38], and complex geometries [39–42]. Recent studies have highlighted the influence of a slowly-varying profile along the channel [43], and of active pumping of the channel walls [44], that lead to a non-trivial dynamics and are useful in controlling the dispersion of solutes in microchannels. Other studies have further addressed active particles and their dispersion in such flows, both theoretically [45–48], and experimentally [49], in an attempt to understand living systems in complex environments in more detail. Even though such a diverse set of theory and modelling has been done, the dynamics of solutes and the modified dispersion when the flow couples to the elasticity of the wall remains an open question. Along the same line, the general coupling between elasto-hydrodynamics and Brownian motion is a recent research topic [50–52].

In this study, we explore the modification induced to Taylor-Aris dispersion when the flow couples to the elasticity of the boundaries for constant and pulsatile pressure at the inlet of an axisymmetric channel. We use the theory of flows in elastic microchannels, by incorporating the elasticity through a Winkler model. The solute transport is described by multiple-time-scale analysis [53, 54] that allows us to describe the long-time dynamics of the cross-sectionally-averaged concentration. We then characterise the changes induced to the advection velocity and dispersion coefficient

---

\* aj756@cam.ac.uk

† thomas.salez@cnrs.fr

due to channel softness. In order to illustrate the main softness-induced effects for practical purposes, we end our discussion by computing the spatiotemporal evolution of a concentration peak of solute under steady flow [55–57].

## II. THEORY

We consider an axisymmetric channel with a wall made of an elastic material, whose elasticity can be modelled as a bed of independent springs, leading to a Winkler law for deformation under applied pressure. A schematic of the system is presented in Fig. 1, where  $a(z, t)$  denotes the local half-radius of the channel that varies along the longitudinal direction  $z$  and time  $t$ . Here,  $a_0$  denotes the radius at the exit and  $l$  denotes the length of the channel. The fluid is assumed to be Newtonian with viscosity  $\eta$  and density  $\rho$ . We consider the hydrodynamic pressure (in excess to the atmospheric one) at the inlet, of amplitude  $p_0$ , to be either steady, or oscillatory with angular frequency  $\omega$ , and the outlet to be open to the atmosphere. The fluid contains a solute, with a diffusion constant  $D$  and a typical concentration  $c_0$ .

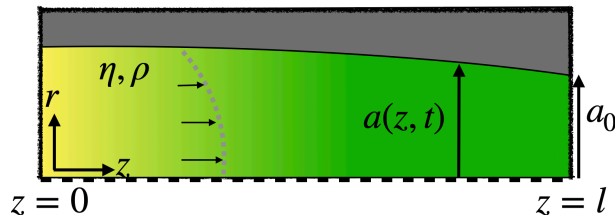


FIG. 1: Schematic of the system under study. We consider a flow of a viscous fluid, with viscosity  $\eta$  and density  $\rho$ , in an elastic, axisymmetric channel. We denote the radial coordinate by  $r$ ,  $r = 0$  corresponding to the revolution axis, and the axial coordinate by  $z$ . The length of the channel is  $l$  and the radius at the exit of the channel is  $a_0$ . The local radius of the channel is denoted by  $a(z, t)$ .

### A. Governing equations

The flow in the channel is governed by the incompressible Navier-Stokes equations with the solute transport described by an advection-diffusion equation. The problem is assumed to be axisymmetric. Hence, the conservation equations for fluid volume, momentum and solute matter are:

$$\frac{\partial u}{\partial z} + \frac{1}{r} \frac{\partial}{\partial r} (rv) = 0, \quad (1)$$

$$\rho \frac{\partial v}{\partial t} + \rho \left( u \frac{\partial v}{\partial z} + v \frac{\partial v}{\partial r} \right) = -\frac{\partial p}{\partial r} + \eta \left[ \frac{\partial^2 v}{\partial z^2} + \frac{1}{r} \frac{\partial}{\partial r} \left( r \frac{\partial v}{\partial r} \right) - \frac{v}{r^2} \right], \quad (2)$$

$$\rho \frac{\partial u}{\partial t} + \rho \left( u \frac{\partial u}{\partial z} + v \frac{\partial u}{\partial r} \right) = -\frac{\partial p}{\partial z} + \eta \left[ \frac{\partial^2 u}{\partial z^2} + \frac{1}{r} \frac{\partial}{\partial r} \left( r \frac{\partial u}{\partial r} \right) \right], \quad (3)$$

$$\frac{\partial c}{\partial t} + u \frac{\partial c}{\partial z} + v \frac{\partial c}{\partial r} = D \left[ \frac{\partial^2 c}{\partial z^2} + \frac{1}{r} \frac{\partial}{\partial r} \left( r \frac{\partial c}{\partial r} \right) \right], \quad (4)$$

where  $v(r, z, t)$ ,  $u(r, z, t)$ ,  $p(r, z, t)$ , and  $c(r, z, t)$  are the radial velocity, axial velocity, hydrodynamic pressure, and concentration fields, respectively. We further assume a no-slip boundary condition at the wall, *i.e.*  $u(r = a, z, t) = 0$ . Hence, fluid volume conservation implies:

$$\frac{\partial(\pi a^2)}{\partial t} + \frac{\partial q}{\partial z} = 0, \quad (5)$$

with the cross-sectional fluid flux defined by:

$$q = 2\pi \int_0^a dr r u. \quad (6)$$

For closure, the constitutive elastic relation between pressure and wall deformation needs to be specified. To this purpose, we assume a Winkler response, *i.e.* a linear and local elastic response where the deformation is proportional

to the pressure [3, 13, 58, 59], as:

$$a = a_0 + kp , \quad (7)$$

where  $k$  is a coefficient (with dimension of a volume per unit force) characterizing the compliance of the wall.

We look for solutions to the equations above under the lubrication approximation, in particular, where  $\epsilon = a_0/l \ll 1$ . At this point, it becomes relevant to look at the various time scales involved in the problem. First, the diffusion time across the channel radius is given by the Taylor time [53, 54, 60]:

$$\tau_0 = \frac{a_0^2}{D} . \quad (8)$$

Second, the advection time across the length of the channel is given by:

$$\tau_1 = \frac{l}{U_0} = \frac{\tau_0}{\text{Pe} \epsilon} , \quad (9)$$

where  $U_0 = p_0 a_0^2 / (l\eta)$  denotes the characteristic fluid velocity scale along the axial direction, and where we introduced the Péclet number  $\text{Pe} = U_0 a_0 / D$ , assumed to be  $O(1)$ . In the specific case of oscillatory flows, we also assume  $\tau_1$  to be comparable to the flow oscillation period  $2\pi/\omega$ . Third, the diffusion time scale across the length of the channel is given by:

$$\tau_2 = \frac{l^2}{D} = \frac{\tau_0}{\epsilon^2} . \quad (10)$$

One thus has the time-scale hierarchy  $\tau_0 \ll t_1 \ll \tau_2$ . In the following, we will ignore the fast dynamics happening at time scales comparable to  $\tau_0$ , since we aim at understanding the concentration evolution on much longer times [53]. Note that we also neglected any viscoelastic and acoustic time scales for the response of the elastic material, as we assumed these to be even smaller than  $\tau_0$ .

Let us now non-dimensionalize the problem through:

$$\begin{aligned} z = lZ , & & r = a_0 R , & & u = U_0 U(R, Z, T) , & & v = \epsilon U_0 V(R, Z, T) , \\ a(z, t) = a_0 A(Z, T) , & & p(r, z, t) = p_0 P(R, Z, T) , & & t = \frac{2\pi}{\omega} T , & & c(r, z, t) = c_0 C(R, Z, T) . \end{aligned}$$

With these scalings, the dimensionless versions of the governing equations read:

$$\frac{\partial U}{\partial Z} + \frac{1}{R} \frac{\partial}{\partial R} (RV) = 0 , \quad (11)$$

$$\frac{\epsilon^2 \text{Wo}^2}{2\pi} \frac{\partial V}{\partial T} + \epsilon^3 \text{Re} \left( U \frac{\partial V}{\partial Z} + V \frac{\partial V}{\partial R} \right) = -\frac{\partial P}{\partial R} + \epsilon^4 \frac{\partial^2 V}{\partial Z^2} + \epsilon^2 \frac{1}{R} \frac{\partial}{\partial R} \left( R \frac{\partial V}{\partial R} \right) - \epsilon^2 \frac{V}{R^2} , \quad (12)$$

$$\frac{\text{Wo}^2}{2\pi} \frac{\partial U}{\partial T} + \epsilon \text{Re} \left( U \frac{\partial U}{\partial Z} + V \frac{\partial U}{\partial R} \right) = -\frac{\partial P}{\partial Z} + \epsilon^2 \frac{\partial^2 U}{\partial Z^2} + \frac{1}{R} \frac{\partial}{\partial R} \left( R \frac{\partial U}{\partial R} \right) , \quad (13)$$

$$\phi \epsilon \frac{\partial C}{\partial T} + \epsilon \text{Pe} \left( U \frac{\partial C}{\partial Z} + V \frac{\partial C}{\partial R} \right) = \frac{1}{R} \frac{\partial}{\partial R} \left( R \frac{\partial C}{\partial R} \right) + \epsilon^2 \frac{\partial^2 C}{\partial Z^2} , \quad (14)$$

$$\text{St} A \frac{\partial A}{\partial T} + \frac{\partial}{\partial Z} \int_0^A dR R U = 0 , \quad (15)$$

$$A = 1 + \kappa P , \quad (16)$$

where we introduced the dimensionless parameter  $\phi = \omega l a_0 / (2\pi D)$ , and the dimensionless compliance  $\kappa = kp_0/a_0$ , and where  $\text{Re} = \epsilon \rho a_0^2 p_0 / \eta^2$ ,  $\text{Wo} = a_0 \sqrt{\rho \omega / \eta}$ , and  $\text{St} = \omega \eta / (2\pi p_0 \epsilon^2)$ , denote the Reynolds, Womersley and Strouhal numbers, respectively. Note that the latter corresponds to the dimensionless expression of  $\tau_1$ .

In the following, we focus on the solutions of the governing equations in the regime where  $\epsilon \ll 1$ ,  $\epsilon \text{Re} \ll 1$ ,  $\epsilon^2 \text{Wo}^2 / (2\pi) \ll 1$ , and  $\text{Pe} \sim O(1)$ . In the specific case of oscillatory flows, we further assume  $\phi \sim O(1)$  and  $\text{St} \sim O(1)$ . Since the flow is independent of the solute concentration dynamics, we address these separately, starting with the former.

## B. Flow profile

The leading-order governing equation for the fluid velocity field reads

$$\frac{\text{Wo}^2}{2\pi} \frac{\partial U}{\partial T} = -\frac{\partial P}{\partial Z} + \frac{1}{R} \frac{\partial}{\partial R} \left( R \frac{\partial U}{\partial R} \right), \quad (17)$$

together with  $\partial P/\partial R = 0$ , and the no-slip boundary condition at the wall  $U(R = A, Z, T) = 0$ .

The steady case (labeled with the “s” subscript) can be described for the flow part by setting  $\text{Wo} = 0$  and  $\text{St} = 0$ , as well as  $T = 0$  (or equivalently dropping the  $T$  variable). Hence, the steady fluid velocity field in the axial direction reads:

$$U_s(R, Z) = \left( \frac{R^2 - A^2}{4} \right) \frac{dP_s}{dZ}, \quad (18)$$

with  $A = 1 + \kappa P_s$ . The mean axial velocity across the cross section is thus given by:

$$\langle U_s \rangle(Z) = \frac{2}{A^2} \int_0^A dR R U_s = -\frac{A^2}{8} \frac{dP_s}{dZ}, \quad (19)$$

where  $\langle \cdot \rangle$  denotes cross-sectional averaging. Furthermore, the steady cross-sectional fluid flux is invariant along the channel axis, leading to:

$$\frac{d}{dZ} \left[ (1 + \kappa P_s)^4 \frac{dP_s}{dZ} \right] = 0. \quad (20)$$

The latter equation, along with the boundary conditions  $P_s(Z = 0) = 1$  and  $P_s(Z = 1) = 0$ , leads to the hydrodynamic pressure field [5, 18]:

$$P_s(Z) = \frac{1}{\kappa} \left( \{ (1 - Z)[(1 + \kappa)^5 - 1] + 1 \}^{1/5} - 1 \right). \quad (21)$$

For the oscillatory case (labeled with the “p” subscript), we assume the axial pressure gradient to be in the form  $\partial P_p/\partial Z = -\mathcal{R}\{G(Z)e^{i2\pi T}\}$ , where  $\mathcal{R}(\cdot)$  denotes the real part and  $G(Z)$  is a complex amplitude to be determined. Correspondingly, the axial velocity field is written as  $U_p = \mathcal{R}\{\tilde{U}_p\}$ , with  $\tilde{U}_p = H(R, Z)e^{i2\pi T}$ , where  $H(R, Z)$  is a complex amplitude to be determined. Doing so, one gets [18, 61]:

$$H(R, Z) = \frac{G(Z)}{i\text{Wo}^2} \left[ 1 - \frac{J_0(i^{3/2}R\text{Wo})}{J_0(i^{3/2}A\text{Wo})} \right], \quad (22)$$

which thus leads to:

$$U_p(R, Z, T) = \mathcal{R} \left\{ \frac{i}{\text{Wo}^2} \left[ 1 - \frac{J_0(i^{3/2}R\text{Wo})}{J_0(i^{3/2}A\text{Wo})} \right] \frac{\partial \tilde{P}_p}{\partial Z} \right\}, \quad (23)$$

where we introduced the complex pressure field  $\tilde{P}_p$ , related to the real one through  $P_p = \mathcal{R}\{\tilde{P}_p\}$ , and the Bessel function of the first kind of order zero  $J_0$ . Then, fluid volume conservation implies:

$$\text{St} A \frac{\partial A}{\partial T} = \mathcal{R} \left\{ \frac{\partial}{\partial Z} \left[ \frac{iA^2}{2\text{Wo}^2} \frac{\partial \tilde{P}_p}{\partial Z} \frac{J_2(i^{3/2}A\text{Wo})}{J_0(i^{3/2}A\text{Wo})} \right] \right\}, \quad (24)$$

where  $J_2$  is the Bessel function of the first kind of order two. Equation (24) together with Eq. (16), *i.e.*  $A = 1 + \kappa \mathcal{R}\{\tilde{P}_p\}$ , and the boundary conditions:

$$\tilde{P}(Z = 0, T) = e^{2\pi i T}, \quad (25)$$

$$\tilde{P}(Z = 1, T) = 0, \quad (26)$$

form a closed set of equations for the pressure that can be solved numerically. Interestingly, due to the elastic coupling in Eq. (16), Eq. (24) is non-linear in the pressure field, and thus expected to generate mode-coupling effects. At small elastic compliance, we can approach the problem analytically with a perturbation expansion in  $\kappa$  [18], as provided in the Appendix.

### C. Solute transport analysis

We employ multiple-time-scale analysis [53, 54, 60] to arrive at the evolution of the cross-sectionally-averaged concentration. Although there are other methods that have been commonly used to study dispersion, including invariant-manifold analysis, method of moments, and others [20, 24, 34, 62, 63], we focus on the multiple-time-scale analysis as it leads to the governing equation for the cross-sectionally averaged concentration dynamics in a way that is convenient for both steady and oscillatory flows. The solute dynamics is given by Eq. (14), together with the solutal no-flux boundary condition at the wall:

$$\left. \frac{\partial C}{\partial R} \right|_{R=A} = \epsilon^2 \left. \frac{\partial A}{\partial Z} \frac{\partial C}{\partial Z} \right|_{R=A} . \quad (27)$$

Following standard multiple-time-scale analysis [64, 65], the time derivative is first expanded as:

$$\frac{\partial}{\partial T} = \frac{\partial}{\partial T_1} + \epsilon \frac{\partial}{\partial T_2} , \quad (28)$$

where  $T_1$  is a “fast” time variable describing dynamics at  $T \sim \omega\tau_1/(2\pi) \sim O(1)$ , and  $T_2$  is a “slow” time variable describing dynamics at  $T \sim \omega\tau_2/(2\pi) \sim O(1/\epsilon)$ . In addition, the concentration field is decomposed as [53, 54, 60]:

$$C(R, Z, T) = \sum_{n=0}^{\infty} \epsilon^n C^{(n)}(R, Z, T_1, T_2) . \quad (29)$$

Substituting the above decompositions in Eqs. (14) and (27), we arrive at the governing equations at different orders in the perturbation parameter  $\epsilon$ . Below, we address these successively up to second order.

#### 1. Leading-order analysis

At  $O(1)$ , the governing equation reads:

$$\frac{1}{R} \frac{\partial}{\partial R} \left( R \frac{\partial C^{(0)}}{\partial R} \right) = 0 , \quad (30)$$

which must satisfy the boundary condition:

$$\left. \frac{\partial C^{(0)}}{\partial R} \right|_{R=A} = 0 . \quad (31)$$

The solution of these two equations indicates that  $C^{(0)}$  is independent of  $R$ . Since the  $O(1)$  solution corresponds in our case to dynamics at times  $T$  much larger than the dimensionless Taylor time  $\omega\tau_0/(2\pi)$ , it is natural to identify  $C^{(0)}$  with the cross-sectionally averaged concentration. This further suggests to impose  $\langle C^{(n)} \rangle = 0$  for  $n > 0$ .

#### 2. First-order analysis

At  $O(\epsilon)$ , the governing equation reads:

$$\phi \frac{\partial C^{(0)}}{\partial T_1} + \text{Pe}U \frac{\partial C^{(0)}}{\partial Z} = \frac{1}{R} \frac{\partial}{\partial R} \left( R \frac{\partial C^{(1)}}{\partial R} \right) , \quad (32)$$

together with the boundary condition:

$$\left. \frac{\partial C^{(1)}}{\partial R} \right|_{R=A} = 0 . \quad (33)$$

Taking the cross-sectional average of the former and using the latter leads to:

$$\phi \frac{\partial C^{(0)}}{\partial T_1} + \text{Pe}\langle U \rangle \frac{\partial C^{(0)}}{\partial Z} = 0 . \quad (34)$$

Combining Eqs. (32) and (34), we arrive at the governing equation for  $C^{(1)}$ , given by:

$$\frac{1}{R} \frac{\partial}{\partial R} \left( R \frac{\partial C^{(1)}}{\partial R} \right) = \text{Pe} (U - \langle U \rangle) \frac{\partial C^{(0)}}{\partial Z} . \quad (35)$$

As such, the axial gradient of  $C^{(0)}$  acts as a source term in the linear differential equation governing the radial variation of  $C^{(1)}$ . Hence, the solution must be in the form:

$$C_s^{(1)} = \text{Pe} N(R, Z) \frac{dC_s^{(0)}}{dZ} \quad (\text{steady flow}) , \quad (36)$$

$$C_p^{(1)} = \text{Pe} \mathcal{R}\{M(R, Z, T_1, T_2)\} \frac{\partial C_p^{(0)}}{\partial Z} \quad (\text{oscillatory flow}) , \quad (37)$$

where the functions  $N(R, Z)$  and  $M(R, Z, T_1, T_2)$  are to be determined.

For the steady case, substituting the above form into the governing equation for  $C^{(1)}$  leads to:

$$\frac{1}{R} \frac{\partial}{\partial R} \left( R \frac{\partial N}{\partial R} \right) = U_s - \langle U_s \rangle . \quad (38)$$

Solving the latter, using Eq. (18), together with the no-flux boundary condition:

$$\left. \frac{\partial N}{\partial R} \right|_{R=A} = 0 , \quad (39)$$

and the vanishing cross-sectional mean, *i.e.*  $\langle N \rangle = 0$ , gives:

$$N = \langle U_s \rangle \left( \frac{R^2}{4} - \frac{R^4}{8A^2} - \frac{A^2}{12} \right) . \quad (40)$$

Similarly, for the oscillatory case, one has:

$$\frac{1}{R} \frac{\partial}{\partial R} \left[ R \frac{\partial (\mathcal{R}\{M\})}{\partial R} \right] = U_p - \langle U_p \rangle . \quad (41)$$

Solving the latter, using Eq. (23), together with the no-flux boundary condition:

$$\left. \frac{\partial M}{\partial R} \right|_{R=A} = 0 , \quad (42)$$

and the vanishing cross-sectional mean, *i.e.*  $\langle M \rangle = 0$ , gives:

$$M(R, Z, T_1, T_2) = \Gamma \frac{\partial \tilde{P}}{\partial Z} \left[ \frac{2}{Aq^3} J_1(qA) - \frac{J_0(qR)}{q^2} + \frac{\beta A^2}{8} - \frac{\beta R^2}{4} \right] , \quad (43)$$

where  $q = i^{3/2} \text{Wo}$ ,  $\Gamma = \frac{1}{i \text{Wo}^2 J_0(qA)}$ , and  $\beta = \frac{2J_1(qA)}{qA}$ .

### 3. Second-order analysis

At  $O(\epsilon^2)$ , the governing equation reads:

$$\phi \frac{\partial C^{(0)}}{\partial T_2} + \phi \frac{\partial C^{(1)}}{\partial T_1} + \text{Pe} U \frac{\partial C^{(1)}}{\partial Z} + \text{Pe} V \frac{\partial C^{(1)}}{\partial R} = \frac{\partial^2 C^{(0)}}{\partial Z^2} + \frac{1}{R} \frac{\partial}{\partial R} \left( R \frac{\partial C^{(2)}}{\partial R} \right) , \quad (44)$$

together with the boundary condition:

$$\left. \frac{\partial C^{(2)}}{\partial R} \right|_{R=A} = \frac{\partial A}{\partial Z} \frac{\partial C^{(0)}}{\partial Z} . \quad (45)$$

The cross-sectional average of the second term on the left-hand side of the governing equation is null, since  $\langle C^{(1)} \rangle = 0$ . Besides, cross-sectional averaging the last term on the right-hand side, and invoking the boundary condition, one has:

$$\left\langle \frac{1}{R} \frac{\partial}{\partial R} \left( R \frac{\partial C^{(2)}}{\partial R} \right) \right\rangle = \frac{2}{A} \frac{\partial A}{\partial Z} \frac{\partial C^{(0)}}{\partial Z}. \quad (46)$$

For steady flows, invoking the first-order results, the cross-sectional averaging of the third and fourth terms on the left-hand side of the governing equation leads to:

$$\text{Pe} \left\langle U_s \frac{\partial C_s^{(1)}}{\partial Z} \right\rangle = \text{Pe}^2 \left( \langle U_s N \rangle \frac{d^2 C_s^{(0)}}{dZ^2} + \left\langle U_s \frac{\partial N}{\partial Z} \right\rangle \frac{dC_s^{(0)}}{dZ} \right), \quad (47)$$

$$\text{Pe} \left\langle V_s \frac{\partial C_s^{(1)}}{\partial R} \right\rangle = \text{Pe}^2 \left\langle V_s \frac{\partial N}{\partial R} \right\rangle \frac{dC_s^{(0)}}{dZ}. \quad (48)$$

Similarly, for oscillatory flows, one has:

$$\text{Pe} \left\langle U_p \frac{\partial C_p^{(1)}}{\partial Z} \right\rangle = \text{Pe}^2 \left( \langle U_p \mathcal{R}\{M\} \rangle \frac{\partial^2 C_p^{(0)}}{\partial Z^2} + \left\langle U_p \mathcal{R} \left\{ \frac{\partial M}{\partial Z} \right\} \right\rangle \frac{\partial C_p^{(0)}}{\partial Z} \right), \quad (49)$$

$$\text{Pe} \left\langle V_p \frac{\partial C_p^{(1)}}{\partial R} \right\rangle = \text{Pe}^2 \left\langle V_p \mathcal{R} \left\{ \frac{\partial M}{\partial Z} \right\} \right\rangle \frac{\partial C_p^{(0)}}{\partial Z}. \quad (50)$$

Combining the averages above, we obtain the general equation:

$$\phi \frac{\partial C^{(0)}}{\partial T_2} + (\text{Pe}^2 \alpha_{s,p} + \alpha_\kappa) \frac{\partial C^{(0)}}{\partial Z} = (1 + \text{Pe}^2 \gamma_{s,p}) \frac{\partial^2 C^{(0)}}{\partial Z^2}, \quad (51)$$

where we introduced the auxiliary functions:

$$\alpha_s = \left\langle U_s \frac{\partial N}{\partial Z} \right\rangle + \left\langle V_s \frac{\partial N}{\partial R} \right\rangle, \quad (52)$$

$$\alpha_p = \left\langle U_p \mathcal{R} \left\{ \frac{\partial M}{\partial Z} \right\} \right\rangle + \left\langle V_p \mathcal{R} \left\{ \frac{\partial M}{\partial R} \right\} \right\rangle, \quad (53)$$

$$\alpha_\kappa = -\frac{2}{A} \frac{\partial A}{\partial Z}, \quad (54)$$

$$\gamma_s = -\langle U_s N \rangle, \quad (55)$$

$$\gamma_p = -\langle U_p \mathcal{R}\{M\} \rangle. \quad (56)$$

We further note that  $\alpha_s = 0$  due to fluid incompressibility, and axial invariance of the cross-sectional fluid flux in the steady case.

Finally, combining Eqs. (28), (34), and (51) leads to the macro-transport equation:

$$\phi \frac{\partial C^{(0)}}{\partial T} + [\text{Pe} \langle U \rangle + \epsilon (\text{Pe}^2 \alpha_{s,p} + \alpha_\kappa)] \frac{\partial C^{(0)}}{\partial Z} = \epsilon (1 + \text{Pe}^2 \gamma_{s,p}) \frac{\partial^2 C^{(0)}}{\partial Z^2}. \quad (57)$$

The latter equation is the central result of the present study. It allows to calculate and understand the influence of the flow-induced deformation of the channel walls on Taylor dispersion. Moreover, we note that the corrections to the advection velocity (proportional to the prefactor of  $\partial C^{(0)}/\partial Z$ ) and dispersion coefficient (proportional to the prefactor of  $\partial^2 C^{(0)}/\partial Z^2$ ) are functions of the axial position  $Z$  for steady flows, and depend on both  $Z$  and  $T$  for oscillatory flows.

### III. DISCUSSION

#### A. Steady flow

We first study the advection velocity and dispersion coefficient in the steady case. Writing the macro-transport equation with dimensional variables, we obtain:

$$\frac{\partial c_s}{\partial t} + \left( \langle u_s \rangle - \frac{2D}{a} \frac{da}{dz} \right) \frac{\partial c_s}{\partial z} = D \left( 1 - \frac{\langle u_s n \rangle}{D^2} \right) \frac{\partial^2 c_s}{\partial z^2}, \quad (58)$$

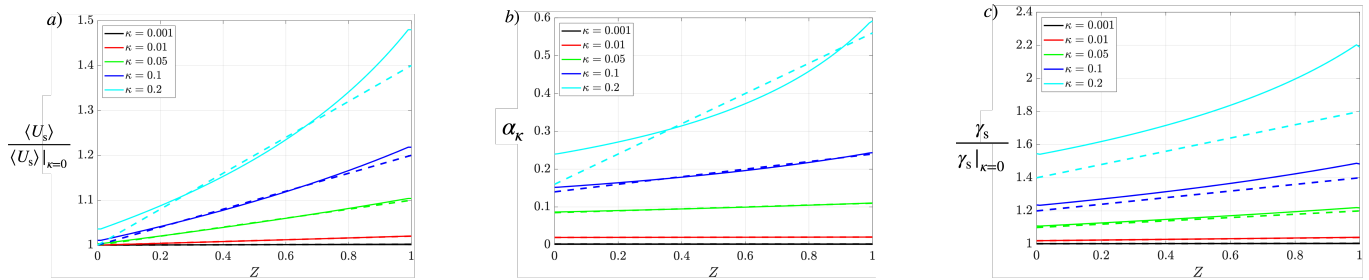


**FIG. 2:** Dimensionless amplification factor  $\langle U_s \rangle / \langle U_s \rangle|_{\kappa=0}$  of the average flow speed (a), dimensionless control factor  $\alpha_\kappa$  of the solutal no-flux contribution to the advection velocity of the solute (b), and solutal-dispersion enhancement factor  $\gamma_s$  (c), as functions of the axial coordinate  $Z$  in the channel, and for various values of the dimensionless compliance  $\kappa$  of the channel wall, as indicated. The solid lines are obtained from Eqs. (59), (60), and (61), respectively. The dashed lines represent the  $O(\kappa^2)$  expansions.

where  $n = U_0 a_0^2 N$ . The general form of the latter equation has been derived in previous works [43, 44] in the context of Taylor dispersion in shaped channels, using heuristic arguments or invariant-manifold theory. The novelty in our case lies in the coupling to the elastic deformations of the channel walls through the combination of the macro-transport equation with Eqs. (7), (19), (21), and (40). Specifically, here, the advection velocity and dispersion coefficient vary along the axis of the channel because of the elastohydrodynamic modification of the channel radius.

Let us first study the advection velocity. It is composed of two separate terms that both depend on the elastic compliance of the wall: i) the first term is the classical cross-sectional average of the flow speed, *i.e.*  $\langle u_s \rangle$ ; ii) the second term,  $-(2D/a)(da/dz)$ , is more subtle and results from the solutal no-flux boundary condition at the deformed wall. The dimensionless amplification factor of the average flow speed, with respect to the rigid case, reads:

$$\frac{\langle U_s \rangle}{\langle U_s \rangle|_{\kappa=0}} = \frac{(\kappa + 1)^5 - 1}{5\kappa \{(\kappa + 1)^5 - [(\kappa + 1)^5 - 1] Z\}^{2/5}} \stackrel{\kappa \rightarrow 0}{\simeq} 1 + 2Z\kappa + (1 - 6Z + 7Z^2)\kappa^2 + O(\kappa^3). \quad (59)$$

Both the full expression and its  $O(\kappa^2)$  expansion are plotted in Fig. 2a). We recover the facts that softer walls induce larger average flow speeds and that the effect monotonically increases along the channel axis, due to larger channel obstruction by elastic deformation [5]. We now turn to the solutal no-flux contribution to the advection velocity. It is null for flat rigid channel walls, and is given by the dimensionless expression  $\epsilon\alpha_\kappa/\text{Pe}$ , where:

$$\alpha_\kappa = -\frac{2[1 - (\kappa + 1)^5]}{5\{(\kappa + 1)^5 - [(\kappa + 1)^5 - 1] Z\}} \stackrel{\kappa \rightarrow 0}{\simeq} 2\kappa + 2\kappa^2(5Z - 3) + O(\kappa^3). \quad (60)$$

Both the full expression and its  $O(\kappa^2)$  expansion are plotted in Fig. 2b). Interestingly, the solutal no-flux contribution at the deformable wall generates a positive increase in the overall advection velocity. Moreover, the magnitude of the effect grows with the dimensionless compliance  $\kappa$ . At  $O(\kappa)$ , the effect is independent of the position  $Z$  along the channel axis, and only at  $O(\kappa^2)$  does this correction begin to monotonically increase along  $Z$ .

Let us now investigate the dispersion part of the problem. The dispersion coefficient takes the Taylor-Aris-like form  $D[1 + \gamma_s \text{Pe}^2]$ , where  $\gamma_s$  controls the magnitude of the flow-induced amplification of axial diffusion. In particular, when  $\kappa = 0$ , we recover the classical Taylor-Aris result,  $\gamma_s = 1/48$ , for rigid cylindrical channels [19, 20]. For soft channels, one further has:

$$\frac{\gamma_s}{\gamma_s|_{\kappa=0}} = \frac{[1 - (\kappa + 1)^5]^2}{25\kappa^2 \{(\kappa + 1)^5 - [(\kappa + 1)^5 - 1] Z\}^{2/5}} \stackrel{\kappa \rightarrow 0}{\simeq} 1 + 2(1 + Z)\kappa + \kappa^2(7Z^2 - 2Z + 3) + O(\kappa^3). \quad (61)$$

Both the full expression and its  $O(\kappa^2)$  expansion are plotted in Fig. 2c). Interestingly, softness generates a positive increase in the dispersion coefficient. Moreover, the magnitude of the effect grows with the dimensionless compliance  $\kappa$  and the axial coordinate  $Z$ . This central result may seem contradictory with the classical Taylor-Aris picture at first sight, since the effective channel radius reduces due to the increasing elastic deformation [5], but is in fact fully consistent with the imposed-pressure configuration and the steady fluid-flux conservation along the channel axis.

## B. Oscillatory flow

Here, we study the advection velocity and dispersion coefficient in the oscillatory case. As in the steady case, they vary along the axis of the channel, but they also depend on time now.

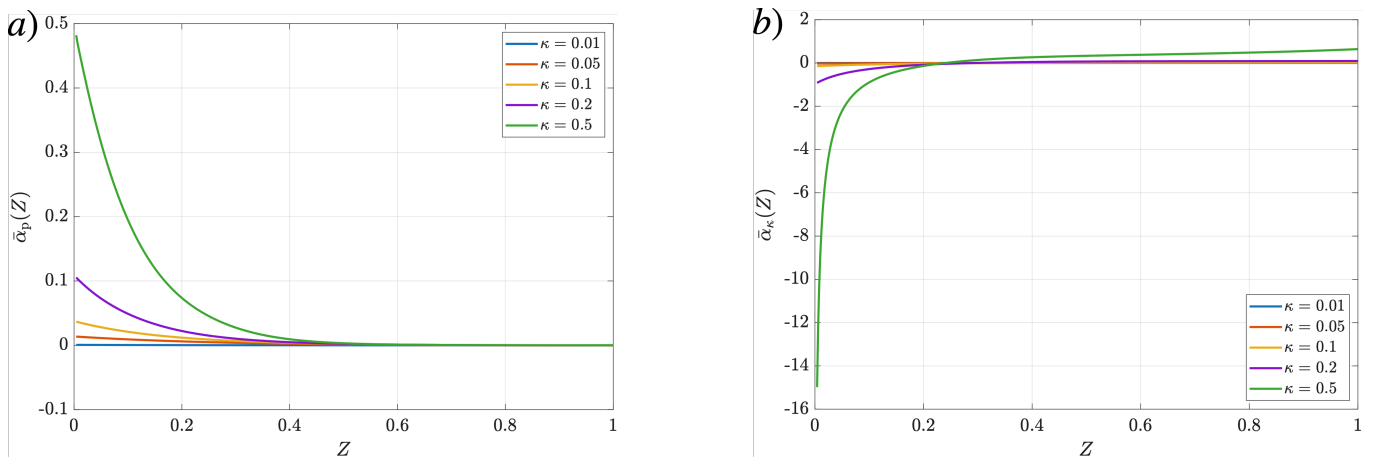


**FIG. 3:** Numerically-computed values of the two dimensionless factors  $\bar{\alpha}_p$  (a) and  $\bar{\alpha}_\kappa$  (b) controlling the period-averaged advection velocity of the solute, as functions of the axial coordinate  $Z$  in the channel, for  $Wo = 1$  and  $St = 2$ , and for various values of the dimensionless compliance  $\kappa$  of the channel wall, as indicated.

Let us first study the advection velocity. In the oscillatory case, one has  $\bar{U}_p = 0$ , where  $\bar{\cdot}$  denotes the average over one oscillation period. The average advection velocity is then composed of two separate terms that both depend on the elastic compliance of the wall, and are controlled by the two dimensionless factors  $\bar{\alpha}_p$  and  $\bar{\alpha}_\kappa$ . Their numerical evaluations are shown in Fig. 3. We observe that  $\bar{\alpha}_p$  is vanishingly small at vanishing compliance. As the compliance increases, the overall magnitude of both factors increases,  $\bar{\alpha}_p$  being positive and monotonically decaying with  $Z$ , and  $\bar{\alpha}_\kappa$  changing sign, from negative to positive, as  $Z$  increases.

Let us now investigate the dispersion part of the problem. The dispersion coefficient is controlled by  $\gamma_p$ . Its numerical evaluation is displayed in Fig. 4, for both  $\gamma_p$  and its period-averaged value, and only shows positive values, which indicates a systematic enhancement of solutal dispersion by the flow, as in classical Taylor-Aris dispersion for a rigid cylindrical channel [19, 20]. In contrast to the latter, dispersion becomes inhomogeneous and complex in the soft case. In particular, most of the effect seems to occur near the channel inlet ( $Z = 0$ ). At the outlet ( $Z = 1$ ), the period-averaged enhancement factor can fall much below the rigid-case value but seems to increase again at the largest  $\kappa$  value. It is important to recall here the elasto-hydrodynamic mode-coupling effect mentioned at the end of Sec. II B. This feature and its consequences can be further understood by performing a perturbation expansion at small compliance, as provided in the Appendix, where the  $O(\kappa)$  pressure field is shown to oscillate with two different frequencies. Since one has  $\gamma_p \sim (\partial P / \partial Z)^2$ , these modes further interact together and generate more harmonics, hence producing a complex overall temporal behaviour.

### C. Implications for solute dispersion

Lastly, we wish to illustrate some practical implications of channel elasticity on solutal dispersion. To do so, we focus on the steady-flow case and compute the solute concentration profile  $C^{(0)}(Z, T)$  over space and time by solving Eq. (57). Note that we are allowed to set  $\phi = 1$  here, despite the fact that  $\omega = 0$  in the steady-flow case. Indeed, a change of time scale in the non-dimensionalization procedure has no influence on the steady flow part of the problem. The results are shown in Fig. 5 and exhibit two main features, in agreement with the above findings. First, the softer the channel, the larger the advection velocity, and thus the earlier the outlet is reached by the concentration peak. Second, the solute disperses more with increasing compliance. Besides the two main points above, an additional feature is that the fore-aft asymmetry in the temporal domain is enhanced at larger compliance.

## IV. CONCLUSION

We investigated theoretically and numerically the Taylor-Aris dispersion in a soft channel, the latter being described by a Winkler elastic model. In particular, using multiple-time-scale analysis, we derived the characteristic macro-transport equation for cross-sectionally-averaged solutal transport, in both steady and oscillatory flows. Our work exhibits the modifications induced by wall elasticity to effective advection velocity and dispersion coefficient. Mainly,

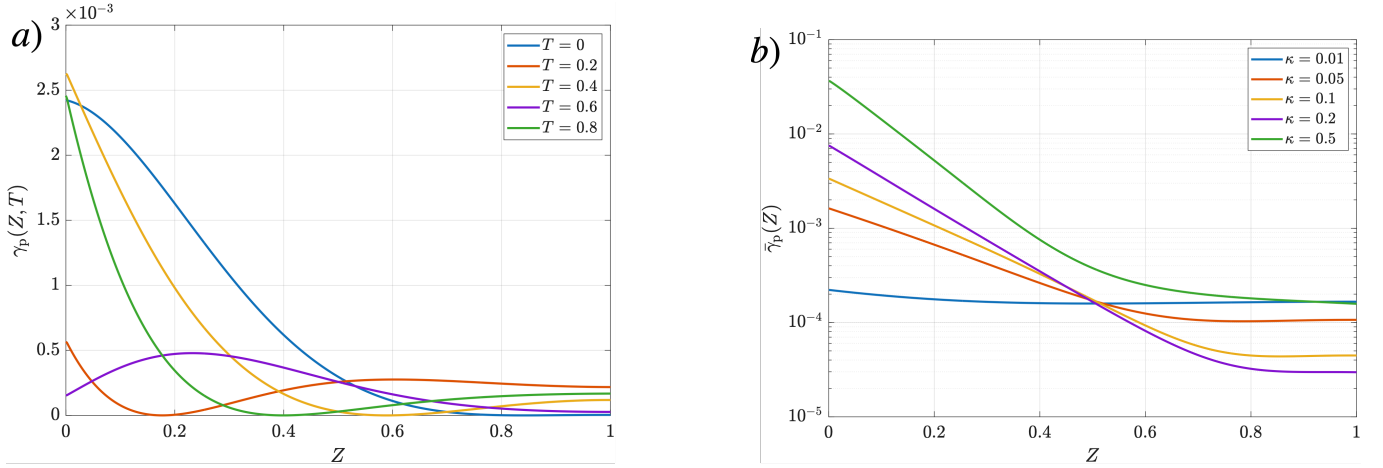


**FIG. 4:** a) Numerically-computed value of the solutal-dispersion enhancement factor  $\gamma_p$ , as a function of the axial coordinate  $Z$  in the channel, for  $Wo = 1$ ,  $St = 2$  and  $\kappa = 0.05$ , and for various dimensionless times  $T$  within one oscillation period, as indicated. b) Corresponding period-averaged solutal-dispersion enhancement factor  $\bar{\gamma}_p$  as a function of the axial coordinate  $Z$  in the channel, for  $Wo = 1$  and  $St = 2$ , and for various values of the dimensionless compliance  $\kappa$  of the channel wall, as indicated.

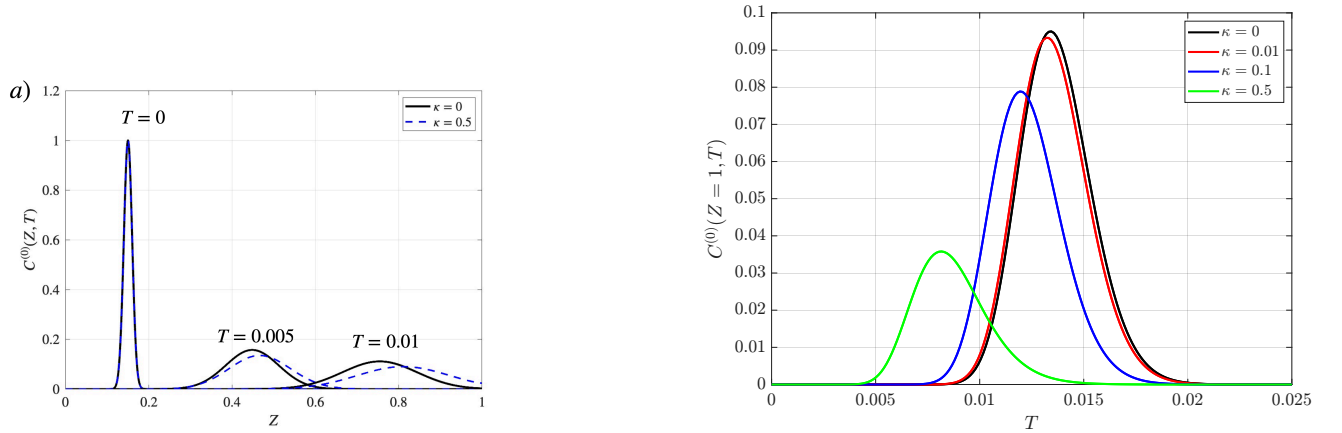


**FIG. 5:** Dimensionless solute concentration profile  $C^{(0)}$  as a function of axial coordinate  $Z$ , for three different dimensionless times  $T$  and two values of the dimensionless compliance  $\kappa$ , as indicated, as obtained from numerically solving Eq. (57) with  $\phi = 1$ ,  $Pe = 500$ ,  $\epsilon = 0.005$ , and using the steady-flow parameters. The initial condition is a Gaussian distribution localised at  $Z = 0.15$  with a standard deviation  $\sigma = 1/(10\sqrt{50})$ . At the channel inlet we apply a full no-flux condition, including both advection and diffusive fluxes, and at the channel outlet we impose  $\partial C^{(0)}/\partial Z = 0$  to allow for the effective solute removal by the flow. b) Dimensionless solute concentration profile  $C^{(0)}$  at the channel outlet ( $Z = 1$ ) as a function of the dimensionless time  $T$ , for various values of the dimensionless compliances  $\kappa$  as indicated.

softness enhances both quantities. This could have direct implications in biology and microfluidic technologies. Beyond these findings, the simulated solutal dynamics in a soft channel offers the possibility to infer the compliance of the channel itself in practice by measuring the distribution of the solute at a given point. This suggests a new non-invasive methodology for the inference of elastic properties of the channel based on standard flow analysis. Specifically, for biomedical applications, this could lead to the development of detection tools for characterising sudden weakening in blood vessels [66], that is one of the major causes of heart diseases. Finally, our work points to several natural extensions. An important next step is to look at diffusio-osmotic and diffusio-phoretic flows in soft channels, where the solute dynamics drives the flow leading to a non-trivial two-way coupling of the elastohydrodynamics and the solute transport. Finally, recent studies on dispersion of active particles have stressed the role of confinement and the current work highlights how wall elasticity could provide a control parameter for the active Taylor-Aris dispersion.

## V. CONFLICTS OF INTEREST

There are no conflicts of interest to declare.

## VI. ACKNOWLEDGMENTS

A.J. thanks the Herchel Smith Fund for a Postdoctoral Fellowship. The authors acknowledge financial support from the Agence Nationale de la Recherche under Softer (ANR21-CE06-0029) and Fricolas (ANR-21-CE06-0039) grants, as well as from the Interdisciplinary and Exploratory Research Program under MISTIC grant at the University of Bordeaux, France. The authors also acknowledge financial support from the European Union through the European Research Council under EMetBrown (ERC-CoG-101039103) grant. Views and opinions expressed are however those of the authors only and do not necessarily reflect those of the European Union or the European Research Council. Neither the European Union nor the granting authority can be held responsible for them. Finally, they thank the RRI Frontiers of Life, which received financial support from the French government in the framework of the University of Bordeaux's France 2030 program, as well as the Soft Matter Collaborative Research Unit, Frontier Research Center for Advanced Material and Life Science, Faculty of Advanced Life Science, Hokkaido University, Sapporo, Japan, and the CNRS International Research Network between France and India on "Hydrodynamics at small scales: from soft matter to bioengineering".

**APPENDIX A: OSCILLATORY FLOW IN A WEAKLY DEFORMABLE CHANNEL**

For a weakly-deformable channel, we approach the problem with a perturbation expansion in  $\kappa$ , through:

$$\tilde{P} = \tilde{P}_0 + \kappa\tilde{P}_1 + O(\kappa^2), \quad (62)$$

as has been done in previous works [9, 14, 15, 18]. At  $O(1)$ , one has:

$$\frac{d^2\tilde{P}_0}{dZ^2} = 0, \quad (63)$$

together with the boundary conditions:

$$\tilde{P}_0(Z = 0, T) = e^{2\pi iT}, \quad (64)$$

$$\tilde{P}_0(Z = 1, T) = 0, \quad (65)$$

which lead to:

$$\tilde{P}_0 = (1 - Z)e^{2\pi iT}. \quad (66)$$

At  $O(\kappa)$ , one has:

$$G_0(\text{Wo}) \frac{\partial^2 \tilde{P}_1}{\partial Z^2} = -\frac{\partial}{\partial Z} \left[ G_1(\text{Wo}) \mathcal{R}\{\tilde{P}_0\} \frac{\partial \tilde{P}_0}{\partial Z} \right] + 2 \text{St} \frac{\partial \tilde{P}_0}{\partial T}, \quad (67)$$

where:

$$G_0(\text{Wo}) = \frac{1}{2i\text{Wo}^2} \frac{J_2(i^{3/2}\text{Wo})}{J_0(i^{3/2}\text{Wo})}, \quad (68)$$

$$G_1(\text{Wo}) = \frac{i}{\text{Wo}^2} \frac{J_1(i^{3/2}\text{Wo})^2}{J_0(i^{3/2}\text{Wo})^2}. \quad (69)$$

All together, these lead to:

$$\tilde{P}_1(Z, T) = \frac{1}{6} Z(1 - Z) \left[ 3 \frac{G_0(\text{Wo})}{G_1(\text{Wo})} \mathcal{R}\{e^{2\pi iT}\} e^{2\pi iT} + (Z - 2) \frac{\text{St}}{G_0(\text{Wo})} 2\pi i e^{2\pi iT} \right]. \quad (70)$$

The real, total pressure field, up to  $O(\kappa)$ , is then given by  $\mathcal{R}\{\tilde{P}_0(Z, T)\} + \kappa\mathcal{R}\{\tilde{P}_1(Z, T)\}$ , where harmonic generation is apparent. In addition, the average of the pressure field over one oscillation period does not vanish at  $O(\kappa)$  [14, 15, 18], and thus generates a streaming flow in the channel.

- 
- [1] Whitesides GM. The origins and the future of microfluidics. *nature*. 2006;442(7101):368-73.
- [2] Stone HA, Kim S. Microfluidics: basic issues, applications, and challenges. *American Institute of Chemical Engineers AIChE Journal*. 2001;47(6):1250.
- [3] Alim K, Andrew N, Pringle A, Brenner MP. Mechanism of signal propagation in *Physarum polycephalum*. *Proceedings of the National Academy of Sciences*. 2017;114(20):5136-41.
- [4] Shapiro M, Brenner H. Taylor dispersion of chemically reactive species: irreversible first-order reactions in bulk and on boundaries. *Chemical engineering science*. 1986;41(6):1417-33.
- [5] Guyard G, Restagno F, McGraw JD. Elastohydrodynamic relaxation of soft and deformable microchannels. *Physical review letters*. 2022;129(20):204501.
- [6] Boyko E, Ilssar D, Bercovici M, Gat AD. Interfacial instability of thin films in soft microfluidic configurations actuated by electro-osmotic flow. *Physical Review Fluids*. 2020;5(10):104201.
- [7] Boyko E, Eshel R, Gat AD, Bercovici M. Nonuniform electro-osmotic flow drives fluid-structure instability. *Physical Review Letters*. 2020;124(2):024501.
- [8] Christov IC. Soft hydraulics: from Newtonian to complex fluid flows through compliant conduits. *Journal of Physics: Condensed Matter*. 2021;34(6):063001.
- [9] Christov IC, Cognet V, Shidhore TC, Stone HA. Flow rate–pressure drop relation for deformable shallow microfluidic channels. *Journal of Fluid Mechanics*. 2018;841:267-86.

- [10] Huang A, Pande SD, Feng J, Christov IC. Oscillatory flows in three-dimensional deformable microchannels. arXiv preprint arXiv:250405132. 2025.
- [11] Martínez-Calvo A, Sevilla A, Peng GG, Stone HA. Start-up flow in shallow deformable microchannels. *Journal of Fluid Mechanics*. 2020;885:A25.
- [12] Anand V, Christov IC. Transient compressible flow in a compliant viscoelastic tube. *Physics of Fluids*. 2020;32(11).
- [13] Wang X, Christov IC. Theory of the flow-induced deformation of shallow compliant microchannels with thick walls. *Proceedings of the Royal Society A: Mathematical, Physical and Engineering Sciences*. 2019;475(2231).
- [14] Rade UM, Pande SD, Christov IC. Theory and simulation of elastoinertial rectification of oscillatory flows in two-dimensional deformable rectangular channels. arXiv preprint arXiv:250522799. 2025.
- [15] Zhang X, Rallabandi B. Elasto-inertial rectification of oscillatory flow in an elastic tube. *Journal of Fluid Mechanics*. 2024;996:A16.
- [16] Boyko E, Christov IC. Non-Newtonian fluid–structure interaction: Flow of a viscoelastic Oldroyd-B fluid in a deformable channel. *Journal of Non-Newtonian Fluid Mechanics*. 2023;313:104990.
- [17] Chun S, Christov IC, Feng J. Experimental investigation of the flow rate–pressure drop relation of a viscoelastic Boger fluid in a deformable channel. *Physical Review Applied*. 2025;24(3):034001.
- [18] Pande SD, Wang X, Christov IC. Oscillatory flows in compliant conduits at arbitrary Womersley number. *Physical Review Fluids*. 2023;8(12):124102.
- [19] Taylor GI. Dispersion of soluble matter in solvent flowing slowly through a tube. *Proceedings of the Royal Society of London Series A Mathematical and Physical Sciences*. 1953;219(1137):186-203.
- [20] Aris R. On the dispersion of a solute in a fluid flowing through a tube. *Proceedings of the Royal Society of London Series A Mathematical and Physical Sciences*. 1956;235(1200):67-77.
- [21] Chatwin P. The approach to normality of the concentration distribution of a solute in a solvent flowing along a straight pipe. *Journal of Fluid Mechanics*. 1970;43(2):321-52.
- [22] Chatwin P. The initial development of longitudinal dispersion in straight tubes. *Journal of Fluid Mechanics*. 1977;80(1):33-48.
- [23] Frankel I, Brenner H. On the foundations of generalized Taylor dispersion theory. *Journal of Fluid Mechanics*. 1989;204:97-119.
- [24] Vedel S, Bruus H. Transient Taylor–Aris dispersion for time-dependent flows in straight channels. *Journal of fluid mechanics*. 2012;691:95-122.
- [25] Vedel S, Hovad E, Bruus H. Time-dependent Taylor–Aris dispersion of an initial point concentration. *Journal of fluid mechanics*. 2014;752:107-22.
- [26] Guyard G, Vilquin A, Sanson N, Jouenne S, Restagno F, McGraw JD. Near-surface rheology and hydrodynamic boundary condition of semi-dilute polymer solutions. *Soft Matter*. 2021;17(14):3765-74.
- [27] Sankarasubramanian R, Gill WN. Unsteady convective diffusion with interphase mass transfer. *Proceedings of the Royal Society of London A Mathematical and Physical Sciences*. 1973;333(1592):115-32.
- [28] Smith R. Effect of boundary absorption upon longitudinal dispersion in shear flows. *Journal of Fluid Mechanics*. 1983;134:161-77.
- [29] Barton N. An asymptotic theory for dispersion of reactive contaminants in parallel flow. *The ANZIAM Journal*. 1984;25(3):287-310.
- [30] Datta S, Ghosal S. Dispersion due to wall interactions in microfluidic separation systems. *Physics of Fluids*. 2008;20(1).
- [31] Levesque M, Bénichou O, Voituriez R, Rotenberg B. Taylor dispersion with adsorption and desorption. *Physical Review E—Statistical, Nonlinear, and Soft Matter Physics*. 2012;86(3):036316.
- [32] Vilquin A, Bertin V, Soulard P, Guyard G, Raphaël E, Restagno F, et al. Time dependence of advection-diffusion coupling for nanoparticle ensembles. *Phys Rev Fluids*. 2021 Jun;6:064201.
- [33] Vilquin A, Bertin V, Raphaël E, Dean DS, Salez T, McGraw JD. Nanoparticle Taylor dispersion near charged surfaces with an open boundary. *Physical review letters*. 2023;130(3):038201.
- [34] Marbach S, Dean DS, Bocquet L. Transport and dispersion across wiggling nanopores. *Nature Physics*. 2018;14(11):1108-13.
- [35] Sarfati R, Calderon CP, Schwartz DK. Enhanced diffusive transport in fluctuating porous media. *ACS nano*. 2021;15(4):7392-8.
- [36] Sharp MK. Shear-augmented dispersion in non-Newtonian fluids. *Annals of biomedical engineering*. 1993;21(4):407-15.
- [37] Rana J, Murthy P. Solute dispersion in pulsatile Casson fluid flow in a tube with wall absorption. *Journal of Fluid Mechanics*. 2016;793:877-914.
- [38] Rana J, Murthy P. Unsteady solute dispersion in non-Newtonian fluid flow in a tube with wall absorption. *Proceedings of the Royal Society A: Mathematical, Physical and Engineering Sciences*. 2016;472(2193):20160294.
- [39] Dorfman KD, Brenner H. Generalized Taylor-Aris dispersion in discrete spatially periodic networks: Microfluidic applications. *Physical Review E*. 2002;65(2):021103.
- [40] Dutta D, Ramachandran A, Leighton Jr DT. Effect of channel geometry on solute dispersion in pressure-driven microfluidic systems. *Microfluidics and Nanofluidics*. 2006;2(4):275-90.
- [41] Dutta D, Leighton DT. Dispersion reduction in pressure-driven flow through microetched channels. *Analytical chemistry*. 2001;73(3):504-13.
- [42] Aminian M, Bernardi F, Camassa R, Harris DM, McLaughlin RM. How boundaries shape chemical delivery in microfluidics. *Science*. 2016;354(6317):1252-6.
- [43] Chang R, Santiago JG. Taylor dispersion in arbitrarily shaped axisymmetric channels. *Journal of Fluid Mechanics*. 2023;976:A30.

- [44] Marbach S, Alim K. Active control of dispersion within a channel with flow and pulsating walls. *Physical Review Fluids*. 2019;4(11):114202.
- [45] Ezhilan B, Saintillan D. Transport of a dilute active suspension in pressure-driven channel flow. *Journal of Fluid Mechanics*. 2015;777:482-522.
- [46] Jiang W, Chen G. Dispersion of active particles in confined unidirectional flows. *Journal of Fluid Mechanics*. 2019;877:1-34.
- [47] Peng Z, Brady JF. Upstream swimming and Taylor dispersion of active Brownian particles. *Physical Review Fluids*. 2020;5(7):073102.
- [48] Jiang W, Chen G. Transient dispersion process of active particles. *Journal of Fluid Mechanics*. 2021;927:A11.
- [49] Lagoin M, Lacherez J, de Tournemire G, Badr A, Amarouchene Y, Allard A, et al. Enhanced dispersion of active microswimmers in confined flows. *Proceedings of the National Academy of Sciences*. 2025;122(50):e2519691122.
- [50] Bickel T. Brownian motion near a liquid-like membrane. *The European Physical Journal E*. 2006;20:379-85.
- [51] Daddi-Moussa-Ider A, Guckenberger A, Gekle S. Particle mobility between two planar elastic membranes: Brownian motion and membrane deformation. *Physics of Fluids*. 2016;28(7).
- [52] Fares N, Lavaud M, Zhang Z, Jha A, Amarouchene Y, Salez T. Observation of Brownian elastohydrodynamic forces acting on confined soft colloids. *Proceedings of the National Academy of Sciences*. 2024;121(42):e2411956121.
- [53] Ng CO. Dispersion in steady and oscillatory flows through a tube with reversible and irreversible wall reactions. *Proceedings of the Royal Society A: Mathematical, Physical and Engineering Sciences*. 2006;462(2066):481-515.
- [54] Chu HC, Garoff S, Przybycien TM, Tilton RD, Khair AS. Dispersion in steady and time-oscillatory two-dimensional flows through a parallel-plate channel. *Physics of Fluids*. 2019;31(2).
- [55] Danckwerts PV. Continuous flow systems. Distribution of residence times. *Chemical engineering science*. 1995;50(24):3857-66.
- [56] Trachsel F, Günther A, Khan S, Jensen KF. Measurement of residence time distribution in microfluidic systems. *Chemical Engineering Science*. 2005;60(21):5729-37.
- [57] Rodrigues AE. Residence time distribution (RTD) revisited. *Chemical engineering science*. 2021;230:116188.
- [58] Gervais T, El-Ali J, Günther A, Jensen KF. Flow-induced deformation of shallow microfluidic channels. *Lab on a Chip*. 2006;6(4):500-7.
- [59] Dendukuri D, Gu SS, Pregibon DC, Hatton TA, Doyle PS. Stop-flow lithography in a microfluidic device. *Lab on a Chip*. 2007;7(7):818-28.
- [60] Fife P, Nicholes K. Dispersion in flow through small tubes. *Proceedings of the Royal Society of London A Mathematical and Physical Sciences*. 1975;344(1636):131-45.
- [61] Womersley J, et al. Oscillatory flow in arteries: the constrained elastic tube as a model of arterial flow and pulse transmission. *Physics in medicine and biology*. 1957;2(2):178-87.
- [62] Mercer GN, Roberts AJ. A centre manifold description of contaminant dispersion in channels with varying flow properties. *SIAM Journal on Applied Mathematics*. 1990;50(6):1547-65.
- [63] Mercer G, Roberts A. A complete model of shear dispersion in pipes. *Japan journal of industrial and applied mathematics*. 1994;11(3):499-521.
- [64] Bender CM, Orszag SA. *Advanced mathematical methods for scientists and engineers: Asymptotic methods and perturbation theory*. vol. 1. Springer; 1999.
- [65] Holmes MH. *Introduction to perturbation methods*. Springer Science & Business Media; 2012.
- [66] Han HC. Twisted blood vessels: symptoms, etiology and biomechanical mechanisms. *Journal of vascular research*. 2012;49(3):185-97.